Computational Materials Science 245 (2024) 113313

Contents lists available at ScienceDirect

Computational Materials Science

journal homepage: www.elsevier.com/locate/commatsci

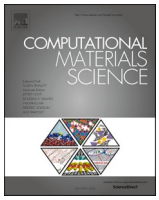

Full Length Article

Pt_3Zr alloy as a protective coating against oxidation and hydrogen attack on Zr-based components in nuclear reactors

J.S. Arellano [a], L.M. Molina [b,*], M.J. López [b], J.A. Alonso [b,c]

[a] Área de Física Atómica Molecular Aplicada (FAMA), CBI, Universidad Autónoma Metropolitana-Azcapotzalco, Av. San Pablo 420, Col. Nueva El Rosario, Ciudad de México, 02128, México
[b] Departamento de Física Teórica, Atómica y Óptica, Universidad de Valladolid, 47011 Valladolid, Spain
[c] Donostia International Physics Center (DIPC), 20018 San Sebastián, Spain

A B S T R A C T

The adsorption of intact and dissociated water molecules on the surfaces of the Pt_3Zr alloy and pure Zr have been investigated by means of density functional theory simulations. In each case, a varying amount of water molecules was placed on the surface until saturation coverage was reached. For both surfaces, all the energy barriers for the partial and complete decomposition of water were calculated. The partial dissociation of H_2O into OH and H, and the complete dissociation into O and two H atoms are significantly more difficult on Pt_3Zr surfaces, as compared to pure Zr surfaces: the dissociative adsorption energies are smaller and the activation barriers for dissociation are larger in Pt_3Zr. In addition, the recombination of H atoms into H_2 molecules and desorption of those molecules is easier on the Pt_3Zr surfaces. The results suggest that the use of the Pt_3Zr alloy as a protective coating in Zr-based metallic components used in nuclear reactors can indeed improve their performance, since the alloyed Pt_3Zr layers are much more resistant towards oxidation and H attack than pure Zr in the presence of hot water vapor.

1. Introduction

Some issues discussed intensively in the literature on nuclear reactors are the oxidation, corrosion and hydrogen diffusion through the surfaces of the vessels and other metallic parts of the nuclear reactors [1,2]. Those problems can give rise to different types of accidents, and even more, to explosions in some nuclear reactors. A very important problem is the corrosion by hot water of the Zr alloys that are used for nuclear fuel cladding [2,3]. Those zirconium alloys were developed, since the 1950 s, not only for their use as nuclear fuel cladding, but also to form part of other nuclear reactor components. They possess important advantages, such as good mechanical properties, low thermal neutron capture cross-section, and corrosion resistance in high temperature water. However, in spite of the advances, the contact of water with the surface of the cladding layer of the nuclear fuel rods is still the main cause of corrosion, and as a consequence hydrogen could enter and diffuse into the alloy [2]. There are evidences that corrosion has a strong dependence on the particular composition of the zirconium alloys. In other words, small changes in the composition and the microstructure of the alloy can lead to significant differences in the resistance to corrosion [4]. The basic corrosion reaction at the surface of the Zr-based alloys is $Zr + 2\,H_2O\,(gas) \rightarrow ZrO_2 + 2\,H_2$, which involves formation of a surface layer of zirconium oxide. The main problem is caused by the hydrogen formed during the oxidation reaction, which can diffuse through the oxide layer and enter inside the alloy, weakening its strength. As a conclusion, water corrosion of zirconium alloy nuclear fuel cladding and the inherent hydrogen pickup into the alloy are potentially limiting factors for the operation of nuclear fuel to high burnup and more extreme conditions. The mechanisms for the oxidation of the surface of Zr metal have been intensively studied [5–10]. Under standard conditions, a layer of ZrO_2 oxide forms on top of the Zr surface, and the presence of this layer does not prevent the diffusion of hydrogen into Zr bulk. The mobility of hydrogen atoms and the increase of their concentration within Zr metal and Zr alloys has also been extensively studied in experimental and theoretical works [11–13].

Two interesting ways of improving the durability of the standard Zr alloys used as cladding for nuclear fuels are either changing their composition, or coating them with thin films of other alloys more resistant to water vapor attack [14–16]. Addition of various dopants can reduce the tendency of the surface towards water adsorption and oxidation. Following this idea, we considered interesting the investigation of the surface properties of the Pt_3Zr alloy, which belongs to the class of so-called ‘superalloys’, characterized by a high degree of chemical ordering and strong stability. At the 3–1 stoichiometry, the very stable compound Pt_3Zr forms, which has the highest melting point (2250 °C) across the Pt-Zr phase diagram [17]. Such high stability and

* Corresponding author.
E-mail address: lmolina@uva.es (L.M. Molina).

https://doi.org/10.1016/j.commatsci.2024.113313
Received 21 March 2024; Received in revised form 18 August 2024; Accepted 19 August 2024
Available online 27 August 2024

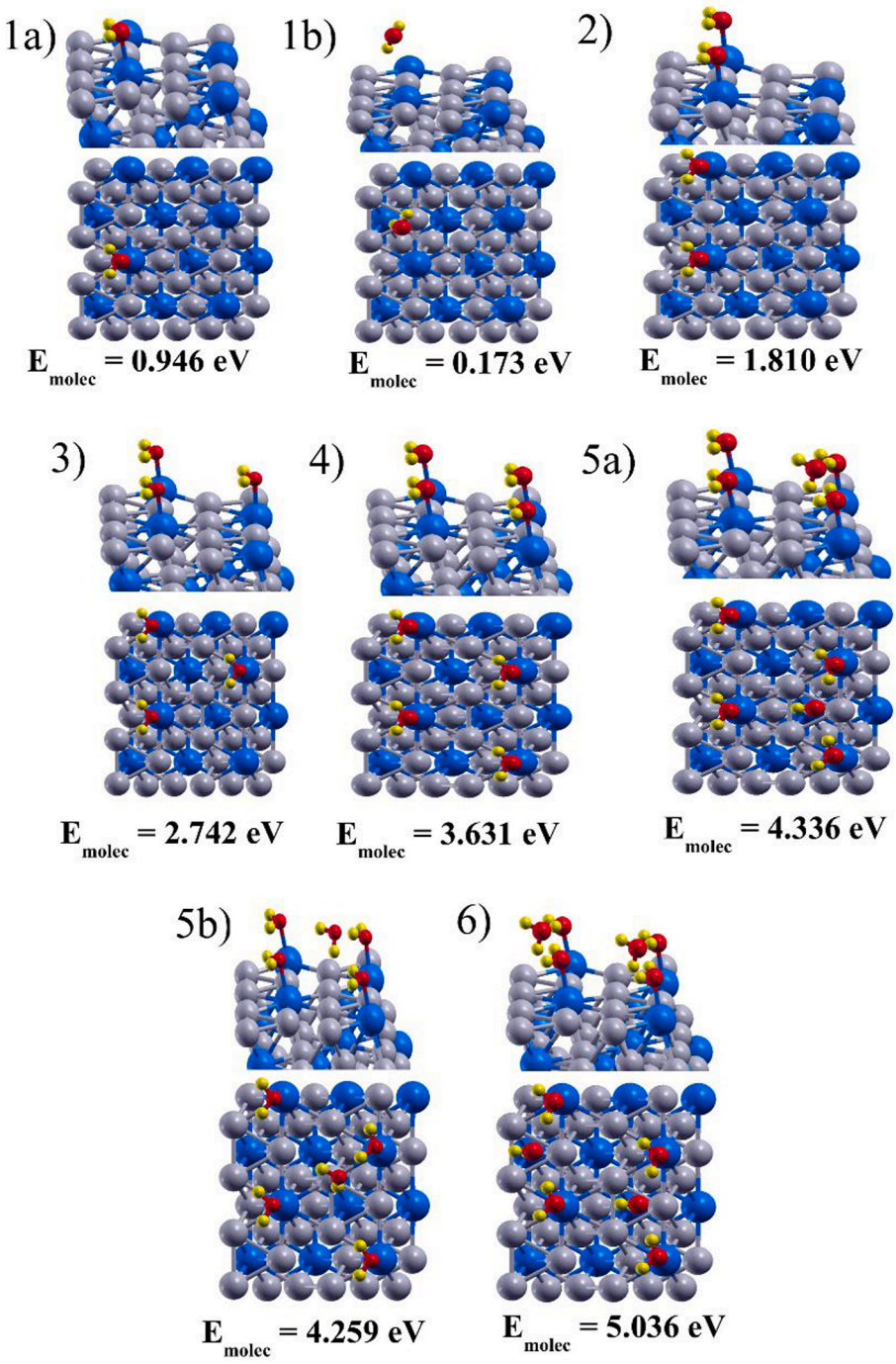

Fig. 1. Top and side views of the lowest energy structures for adsorption of one to six water molecules at the Pt_3Zr surface. In each case, the total adsorption binding energy $E_{molec}[nH_2O]$ of the n molecules is given. One low lying configuration is also given in the cases of one and five adsorbed molecules. Gray spheres: Pt atoms. Blue spheres: Zr atoms. Red spheres: O atoms. Yellow spheres: H atoms.

melting point make this material very interesting for its potential use as coating of the zirconium alloys employed in nuclear reactors. Some experimental and theoretical work has been done on the surface and bulk properties of this alloy. Pan et al. [18] studied the electronic structure of this compound and the energetics of oxygen insertion into the bulk of the alloy. Experiments by Li et al. [19] examined the structure and adhesion properties of thin films of zirconium oxide grown on top of the Pt_3Zr alloy. A study by Antlanger et al. [20] investigated pure and oxidized Pt_3Zr (0001) surfaces by scanning tunneling microscopy (STM), Auger electron spectroscopy, and density functional theory (DFT). The experimental work of Lackner et al. [21] analyzed the interaction of water with thin layers of ZrO_2 grown on top of the Pt_3Zr alloy. DFT simulations by Ruiz Puigdollers et al. [22] focussed on the reducibility of those thin ZrO_2 layers and their interaction with hydrogen.

In this manuscript, we report the results of an extensive comparison, using the density functional formalism [23], of the interaction of water with pure Zr and Pt_3Zr surfaces. In each case, we analyze the interaction of water with those surfaces at various water coverages, and with the water molecules either intact, partially dissociated into H atoms and hydroxyl OH groups, or completely dissociated into O and H atoms. The activation barriers for dissociation were calculated. Also, we have

Table 1
Average adsorption energies per molecule, $E^{av}_{molec}[nH_2O]$, for adsorption of $n = 1$ – 6 water molecules (per unit cell) on the Pt_3Zr surface, and adsorption energy of each newly added molecule, $E^{last}_{molec}[nH_2O]$. All energies in eV.

n	1	2	3	4	5	6
$E^{av}_{molec}[nH_2O]$	0.946	0.905	0.914	0.908	0.867	0.839
$E^{last}_{molec}[nH_2O]$	0.946	0.864	0.932	0.889	0.705	0.777

simulated the adsorption of several oxygen atoms at each of the two surfaces, to gain some understanding on the initial processes leading towards surface oxidation. The results show that the Pt_3Zr surface is indeed much less reactive than the pure Zr surface. Therefore, we expect that coating Zr-based alloys with thin layers of Pt_3Zr can significantly improve the durability of these materials as nuclear fuel cladding.

2. Computational details

Electronic structure calculations were performed using Density Functional Theory (DFT) [23] and the gradient-corrected GGA-PBE exchange–correlation functional [24]. The Projected Augmented Wave (PAW) technique was used, as implemented in the GPAW code [25]. This method is based on the use of a real space three-dimensional grid (with a uniform grid spacing of 0.2 Å in our case) to sample the electronic wave functions. Scalar-relativistic pseudopotentials were employed to describe the interaction between core and valence electrons. For the H, O, Pt and Zr atoms, 1, 6, 10 and 12 valence electrons are considered, respectively. In the case of Zr, including 4*s* and 4*p* electrons as valence electrons is necessary in order to prevent errors due to core-polarization.

The simulations of adsorption of water on the pure Zr and Pt_3Zr surfaces were performed using a slab model with a thickness of four atomic layers. The atoms in the bottom two layers were kept fixed at their positions in the bulk, and the two upper layers were freely relaxed under the presence of the adsorbates. To ensure that the wave functions decay to very small values at the *z*-direction boundary of the unit cell, a vacuum space of 14 Å was taken in the *z* direction on top of the slab. To be able to simulate a sizable coverage of intact and dissociated water molecules, a large lateral (in the *x* and *y* directions) unit cell of size 9.97 Å × 11.52 Å was employed for the Pt_3Zr surface. In the case of pure Zr,

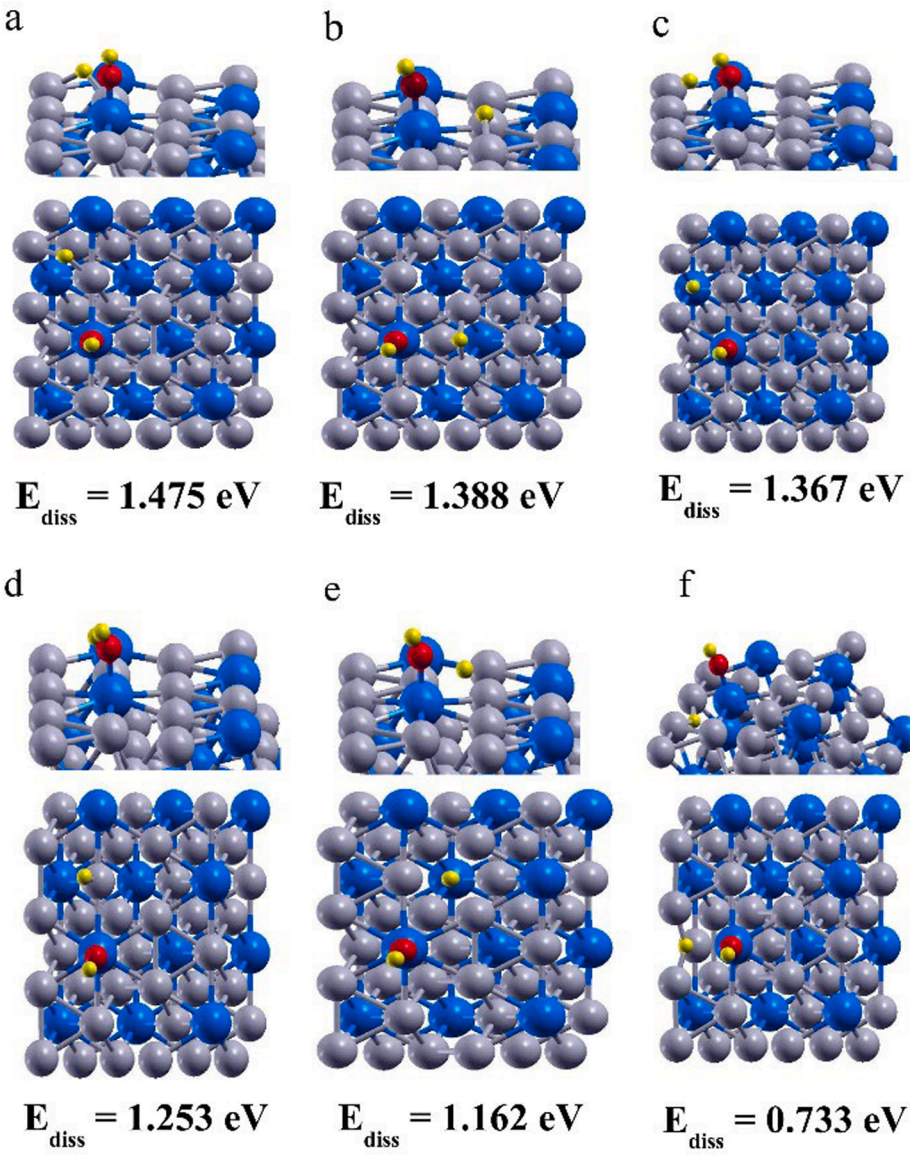

Fig. 2. Top and side views of the relaxed structures for several adsorption configurations of a single water molecule dissociated into OH and H at the Pt_3Zr surface. In each case, the adsorption energy $E_{diss}[OH+H]$ (see eq. (5)) is given.- Gray spheres: Pt atoms. Blue spheres: Zr atoms. Red spheres: O atoms. Yellow spheres: H atoms.

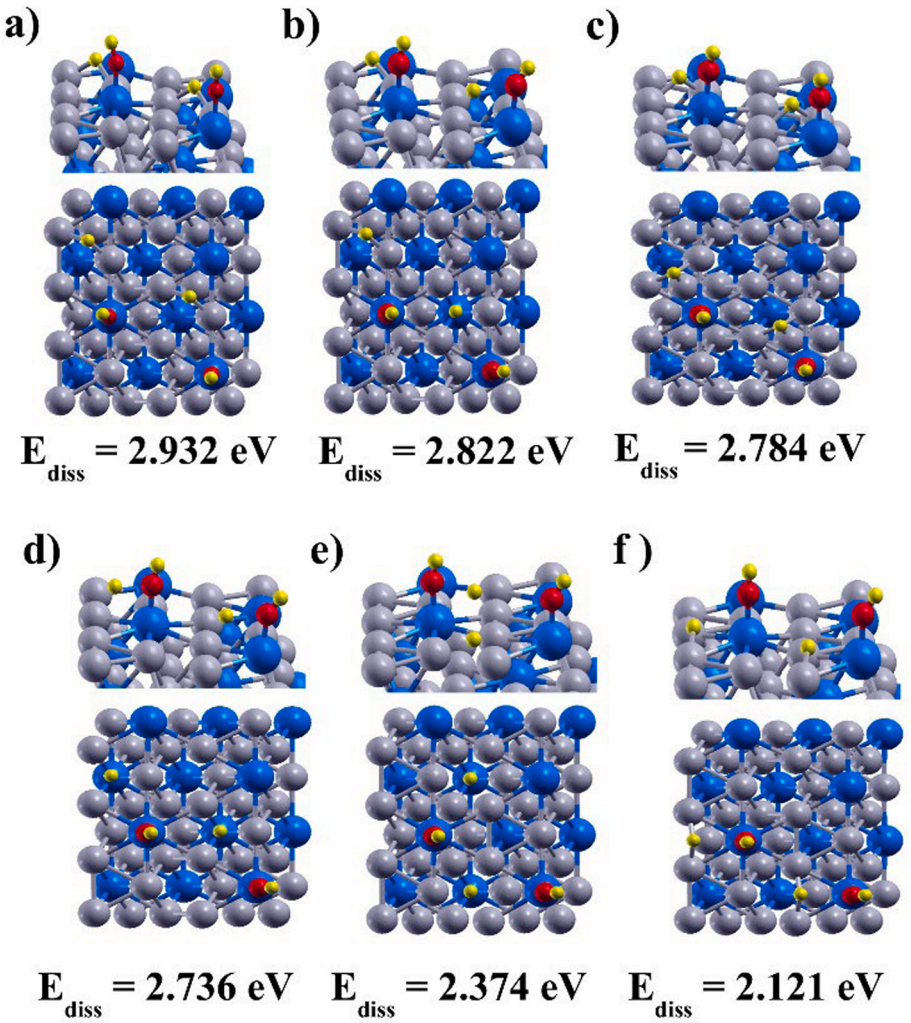

Fig. 3. Top and side views of the relaxed structures for several adsorption configurations of two water molecules dissociated into OH and H at the Pt_3Zr surface. In each case, the total adsorption energy $E_{diss}[2(OH+H)]$ (with respect to two gas phase H_2O molecules) is given.- Gray spheres: Pt atoms. Blue spheres: Zr atoms. Red spheres: O atoms. Yellow spheres: H atoms.

the size of the unit cell size in the *x* and *y* directions was 11.22 Å × 12.96 Å. In both cases, those unit cells consist of 16 surface sites. Such large unit cells allow us simulating both the adsorption of isolated water molecules, and the co-adsorption of several water molecules, hydroxyls, etc., with the intention of studying the saturation coverage for each adsorbed species. A Monkhorst-Pack sampling of 2 × 2 *k*-points was found sufficient to obtain binding energies converged within 0.01 eV. Geometries were relaxed using the Broyden–Fletcher–Goldfarb–Shanno (BFGS) algorithm [26], until the maximum force on any atom was smaller than 0.015 eV/Å. This procedure results in total energies converged within 0.001 eV. Energy barriers for water dissociation were calculated using a constrained minimization method, involving several simulations where the reaction coordinate (the O–H bond distance) was restricted at monotonously increasing values, while allowing the rest of the system to freely relax [27]. For each of the two surfaces (pure Zr and the Pt_3Zr alloy) we simulate the adsorption of a varying number of water molecules, either intact, partially dissociated into H and OH, or completely dissociated into co-adsorbed O and H atoms. For each of those cases, water molecules are successively adsorbed until signs of saturation coverage appear. This will happen when the binding energy of the last adsorbed molecule shows a sizable decrease.

The dependence of the results with respect to the number of substrate layers used in the calculations has been analyzed by performing selected calculations with three, four, five and six layers in the substrate, with the positions of the atoms of the two bottom layers fixed in all cases. Table S1 of the Supplementary Material shows that the convergence of the molecular (H_2O) and dissociative (OH+H) adsorption energies with the number of substrate layers is fast, and that using four layers is quite enough to get accurate results. Other workers have used substrates with three or four layers to study the behavior of gases on the surface of transition metals [28–30].

3. Results and discussion

3.1. Water on the Pt_3Zr surface

We first discuss the adsorption of water on the $Pt_3Zr(0001)$ surface, at increasing coverage. All possible adsorption sites were explored, and the structures were relaxed. Fig. 1 shows top and side views of the lowest energy structures for the adsorption of up to six intact (non-dissociated) water molecules in the unit cell. The total binding energies for molecular adsorption of *n* non-dissociated water molecules

$$E_{molec}[nH_2O] = nE[H_2O\ \text{gas}] + E[\text{surface}] - E[nH_2O\ \text{on surface}] \quad (1)$$

obtained by subtracting the total energy of the system with *n* adsorbed molecules from the sum of the energies of *n* water molecules in the gas phase and the energy of the clean surface, are also given in Fig. 1. The positive values of $E_{molec}[nH_2O]$ indicate that the process is exothermic.

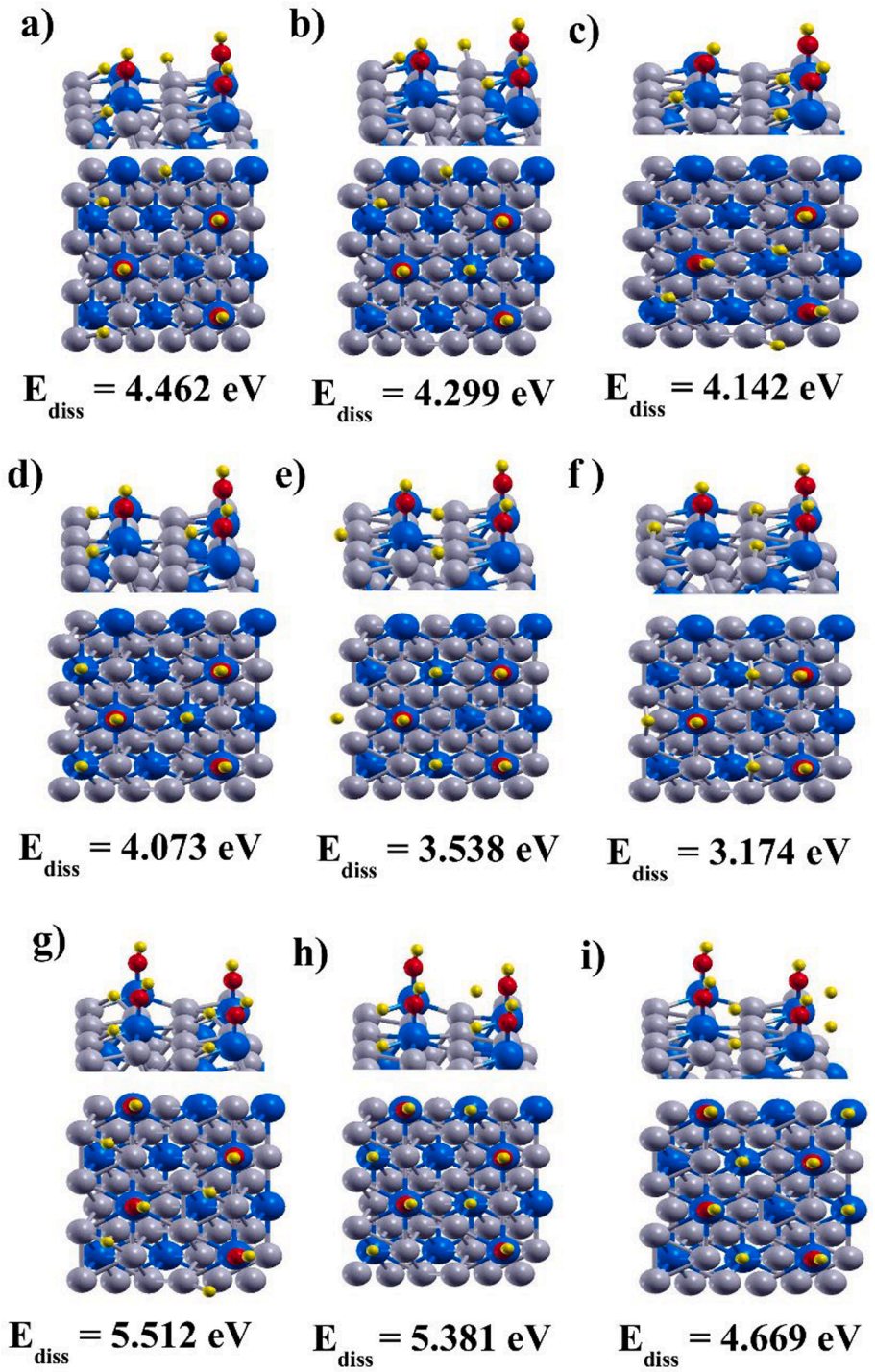

Fig. 4. Top and side views of the relaxed structures for several adsorption configurations of three (panels a to f) and four (panels g to i) water molecules dissociated into OH groups and H atoms at the Pt_3Zr surface. In each case, the total dissociative adsorption energies $E_{diss}[3(OH+H)]$ and $E_{diss}[4(OH+H)]$, with respect to three and four gas phase H_2O molecules, respectively, are given.- Gray spheres: Pt atoms. Blue spheres: Zr atoms. Red spheres: O atoms. Yellow spheres: H atoms.

Table 1 gives the average adsorption energies per molecule,

$$E^{av}_{molec}[nH_2O] = E_{molec}[nH_2O]/n \tag{2}$$

and the incremental binding energy, that is, the adsorption energy of the last adsorbed molecule (this is the energy released upon adsorption of the last water molecule on the surface)

$$E^{last}_{molec}[nH_2O] = E[H_2O \text{ gas}] + E[(n-1)H_2O \text{ on surface}] - E[nH_2O \text{ on surface}]. \tag{3}$$

The adsorption energy of the last adsorbed molecule can alternatively be calculated as the difference

$$E^{last}_{molec}[nH_2O] = E_{molec}[nH_2O] - E_{molec}\left[(n-1)H_2O\right]. \tag{4}$$

A single water molecule adsorbs on top of a Zr atom, with the molecular plane almost parallel to the surface and the oxygen atom attached to Zr (see Fig. 1). The adsorption binding energy is 0.95 eV, revealing that the interaction between O and Zr is strong. When the water molecule is initially placed on top of a Pt atom, the O-Pt interaction becomes

Table 2
Average adsorption energy per molecule, $E^{av}_{diss}[n(OH+H)]$ for the dissociative adsorption of $n = 1 - 4$ water molecules into OH and H on the Pt_3Zr surface, and dissociative adsorption energy of each newly added water molecule, $E^{last}_{diss}[n(OH+H)]$. All energies in eV. Starting at $n = 4$, the favorable sites for H adsorption saturate, and the dissociative adsorption energy of the last water molecule decreases appreciably.

n	1	2	3	4
$E^{av}_{diss}[n(OH+H)]$	1.475	1.466	1.487	1.378
$E^{last}_{diss}[n(OH+H)]$	1.475	1.457	1.530	1.050

unfavorable, and the water molecule rotates until it forms a weak H-Pt bond (panel 1b). This configuration is much less stable, with a binding energy of 0.17 eV. Therefore, for multiple H_2O adsorption, it makes sense to occupy all available surface Zr sites. The total adsorption energy increases linearly with the number of adsorbed molecules, at a rate of approximately 0.9 eV per H_2O molecule, for adsorption from one up to four water molecules. This is not surprising, since the mutual distance between adsorbed water molecules is relatively large, making the adsorption of each additional molecule independent from the previous ones. Since we use a 2×2 unit cell, the four Zr surface sites become

Table 3
Average adsorption energy per molecule, $E^{av}_{diss}[n(O+H+H)]$ for the dissociative adsorption of $n = 1 - 3$ water molecules into O and two H atoms on the Pt_3Zr surface, and dissociative adsorption energy of each newly added water molecule, $E^{last}_{diss}[n(O+H+H)]$. All energies in eV.

n	1	2	3
$E^{av}_{diss}[n(O+H+H)]$	1.329	1.096	0.793
$E^{last}_{diss}[n(O+H+H)]$	1.329	0.864	0.185

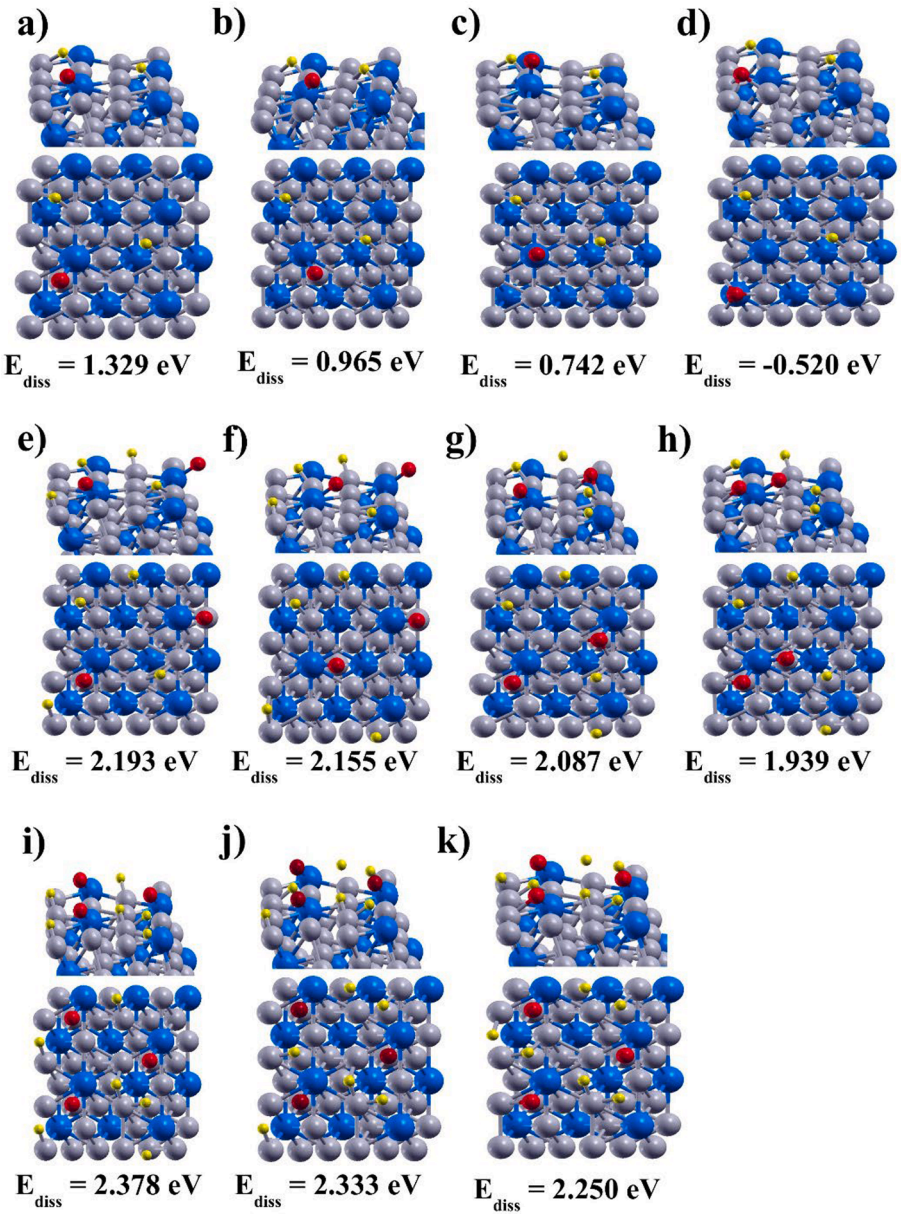

Fig. 5. Top and side views of the relaxed structures for several adsorption configurations with one (conformers a, b, c, d), two (conformers e, f, g, h), and three (conformers i, j, k) water molecules (per unit cell) fully dissociated into O and H atoms at the Pt_3Zr surface. In each case, the total dissociative adsorption energy $E_{diss}[n(O+H+H)]$ with respect to n gas phase molecules ($n = 1, 2, 3$) is given.- Gray spheres: Pt atoms. Blue spheres: Zr atoms. Red spheres: O atoms. Yellow spheres: H atoms.

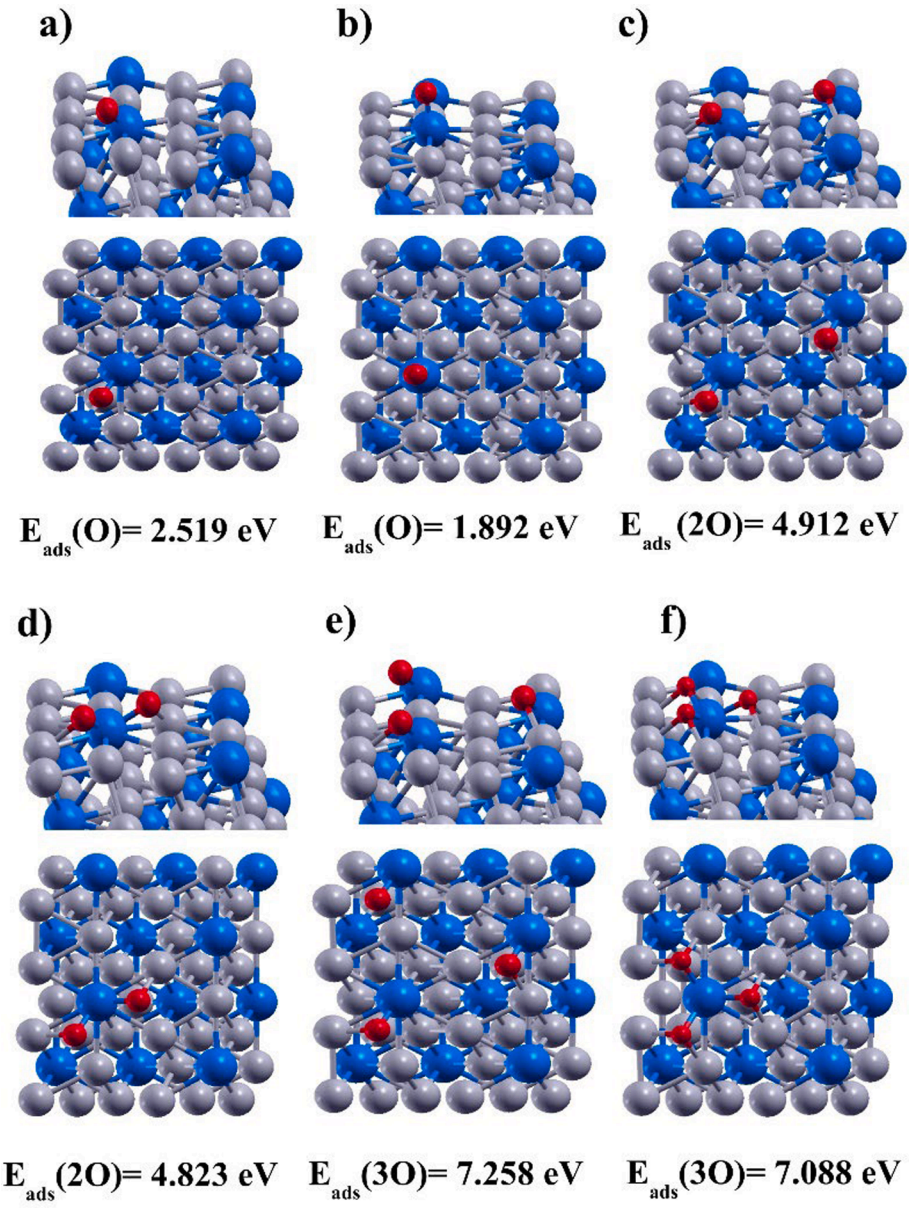

Fig. 6. Top and side views of the relaxed structures for adsorption of one, two and three oxygen atoms at the Pt_3Zr surface. The lowest energy configuration and a low-lying structure are shown in each case. The total adsorption energies of the n oxygen atoms, $E_{ads}[nO]$, defined in eq. (11), are given.- Gray spheres: Pt atoms. Blue spheres: Zr atoms. Red spheres: O atoms. Yellow spheres: H atoms.

Table 4
Desorption energies $E_{desorp}[nH_2]$ required to recombine the H atoms into H_2 molecules and desorb those molecules from a Pt_3Zr surface covered with n fully dissociated water molecules ($n = 1$–3) on the oxidized nO-Pt_3Zr surface. Energies in eV.

n	1	2	3
$E_{desorp}[nH_2]$	1.313	2.286	2.628
$E^{av}_{desorp}[nH_2]$	1.313	1.143	0.876

saturated after the adsorption of four H_2O molecules. So, the fifth H_2O molecule is adsorbed on top of a Pt atom. Although some stability is gained by forming hydrogen bonds with neighbor water molecules, the impossibility of forming an O-Zr bond causes a drop in the adsorption binding energy, from 0.90 eV for the fourth molecule to 0.70 eV for the fifth one. The sixth water molecule also binds in a similar conformation, involving hydrogen bonds with co-adsorbed water molecules.

The dissociative adsorption of water molecules into OH and H at the Pt_3Zr surface has been studied next. Similar to equations (1), (2), and (3), total dissociative adsorption energies of n water molecules per unit cell

$$E_{diss}[n(OH+H)] = E[nH_2O \text{ gas}] + E[\text{surface}] - E[n(OH+O) \text{ on surface}] \quad (5)$$

average dissociative adsorption energies

$$E^{av}_{diss}[n(OH+H)] = E_{diss}[n(OH+H)]/n \quad (6)$$

and the dissociative adsorption energy of the last water molecule

$$E^{last}_{diss}[n(OH+H)] = E[H_2O \text{ gas}] + E[(n-1)(OH+H) \text{ on surface}] - E[n(OH+H) \text{ on surface}] \quad (7)$$

can be defined. The structures for several optimized configurations of

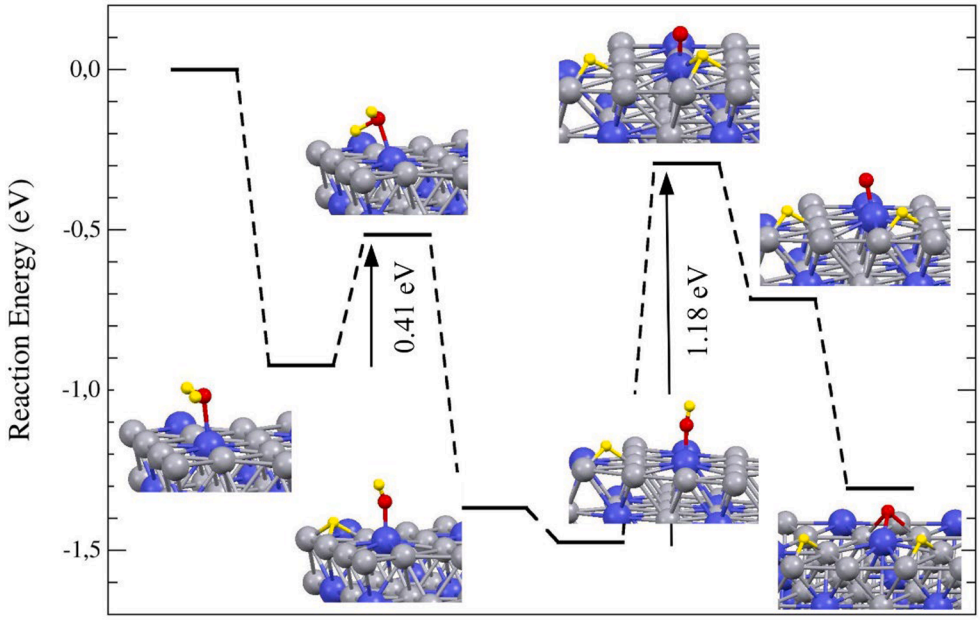

Fig. 7. Intermediate steps and reaction barriers for the dissociation of H_2O into adsorbed O and H atoms at the Pt_3Zr surface. Zero energy corresponds to the Pt_3Zr surface and a free H_2O molecule.

one dissociated molecule are shown in Fig. 2. As expected, the OH group has a strong preference to bind on top of the Zr atoms, forming a strong O-Zr bond with bond-length of 1.91 Å. The corresponding dissociative adsorption energies $E_{diss}[OH+H]$ are also given in Fig. 2. It should be noticed that the reference is formed by a gas water molecule and the pristine surface. In the most stable configuration (conformer a in Fig. 2) the dissociative adsorption energy is 1.475 eV, around 0.5 eV higher than the adsorption energy of intact H_2O. In this dissociated configuration, the H atom binds at a Pt-Pt bridge site, at distances 1.80 and 1.81 Å from the two Pt atoms. When the H atom sits at other Pt-Pt bridge sites (conformer b), or at hollow sites between three Pt atoms (conformers c and e), the dissociative adsorption energies decrease by 0.1-–0.3 eV. The possibility of placing the H atom at a location below the surface was also explored. In conformer f the H atom is embedded slightly below the surface, 0.45 Å below the most external layer of Pt atoms, and that configuration is less stable than conformer a by 0.7 eV.

Fig. 3 shows several configurations for the co-adsorption of two dissociated water molecules at the Pt_3Zr surface. The most stable configuration occurs when each dissociated molecule is adsorbed in the same conformation as in the most stable case of a single dissociated H_2O molecule (see Fig. 2a). The total dissociative adsorption energy of the two molecules, $E_{diss}[2(OH+H)] = 2.932$ eV, almost coincides with twice the dissociative adsorption energy of a single molecule ($E_{diss}[OH+H] = 1.475$ eV), because the distance between the co-adsorbed molecules is relatively large. This means that, at this stage, coverage is still sparse and there are no competitive co-adsorption effects. Again, attaching the H atoms to other Pt-Pt bridge sites (see conformers 3b and 3c) results in a reduction of the total adsorption energy by 0.1-–0.2 eV. It is interesting to compare configurations 3d and 3e. In these, the H atoms occupy different types of hollow sites between three Pt atoms, and configuration 3d is clearly preferred over 3e. In the first case, the hollow site has a Zr atom right below it in the second layer, whereas in the second case the hollow site has an empty space below in the second layer. The results for three and four dissociated H_2O molecules are shown in Fig. 4. For three molecules (configurations a to f), there is just enough room on the surface to place the three H atoms at the most favorable binding sites, and therefore the total adsorption energy $E_{diss}[3(OH+H)]$ is approximately equal to three times the dissociative adsorption energy of a single molecule. Starting at four water molecules (configurations g-i), saturation effects begin to appear. In the most stable conformation, the dissociative adsorption energy of the fourth water molecule is $E^{last}_{diss}[4(OH+H)] = 1.0$ eV, while for the third molecule $E^{last}_{diss}[3(OH+H)]$ it was around 1.4 eV (see Table 2).

Finally, the complete dissociative adsorption of water molecules into O and two H atoms on the surface of Pt_3Zr has been investigated, and the geometries for several adsorption configurations are shown on Fig. 5 for one (conformers a, b, c, d), two (conformers e, f, g, h), and three (conformers i, j, k) molecules. Those conformers include the lowest energy configuration and several low-lying structures. As expected, H atoms prefer to bind at Pt-Pt bridge sites as in the case of OH+H. Oxygen atoms occupy hollow sites between two Pt atoms and a Zr atom. The adsorption energies for full dissociation of the water molecules are defined

$$E_{diss}[n(O+H+H)] = E[nH_2O\,\text{gas}] + E[\text{surface}] - E[n(O+H+H)\,\text{on surface}] \tag{8}$$

$$E^{av}_{diss}[n(O+H+H)] = E_{diss}[n(O+H+H)]/n \tag{9}$$

$$E^{last}_{diss}[n(O+H+H)] = E[H_2O\,\text{gas}] + E[(n-1)(O+H+H)\,\text{on surface}] - E[n(O+H+H)\,\text{on surface}] \tag{10}$$

For a single water molecule per unit cell, the dissociated adsorption energy, $E_{diss}[O+H+H] = 1.329$ eV, is a bit smaller than the adsorption energy corresponding to the dissociation into OH and H, $E_{diss}[OH+O] = 1.475$ eV. This means that splitting the adsorbed OH group into O and H atoms on the Pt_3Zr surface has an energy cost of 0.15 eV. Configuration d in Fig. 5 reveals that the stability drops drastically when the O atom does not make contact with a surface Zr atom. In fact, that structure becomes thermodynamically unstable. Table 3 shows the evolution of the dissociative adsorption energies with the number of adsorbed water molecules. Strong competitive effects begin to appear at $n = 2$, with E_{diss} and E^{last}_{diss} decreasing markedly. This means that the presence of co-adsorbed H atoms causes a lowering in the ability of the Pt_3Zr surface to catalyze the dissociation of additional water molecules.

For completeness, Fig. 6 shows the structures corresponding to adsorption of oxygen atoms at the Pt_3Zr surface. The lowest energy configuration and a low-lying structure are given for one, two and three

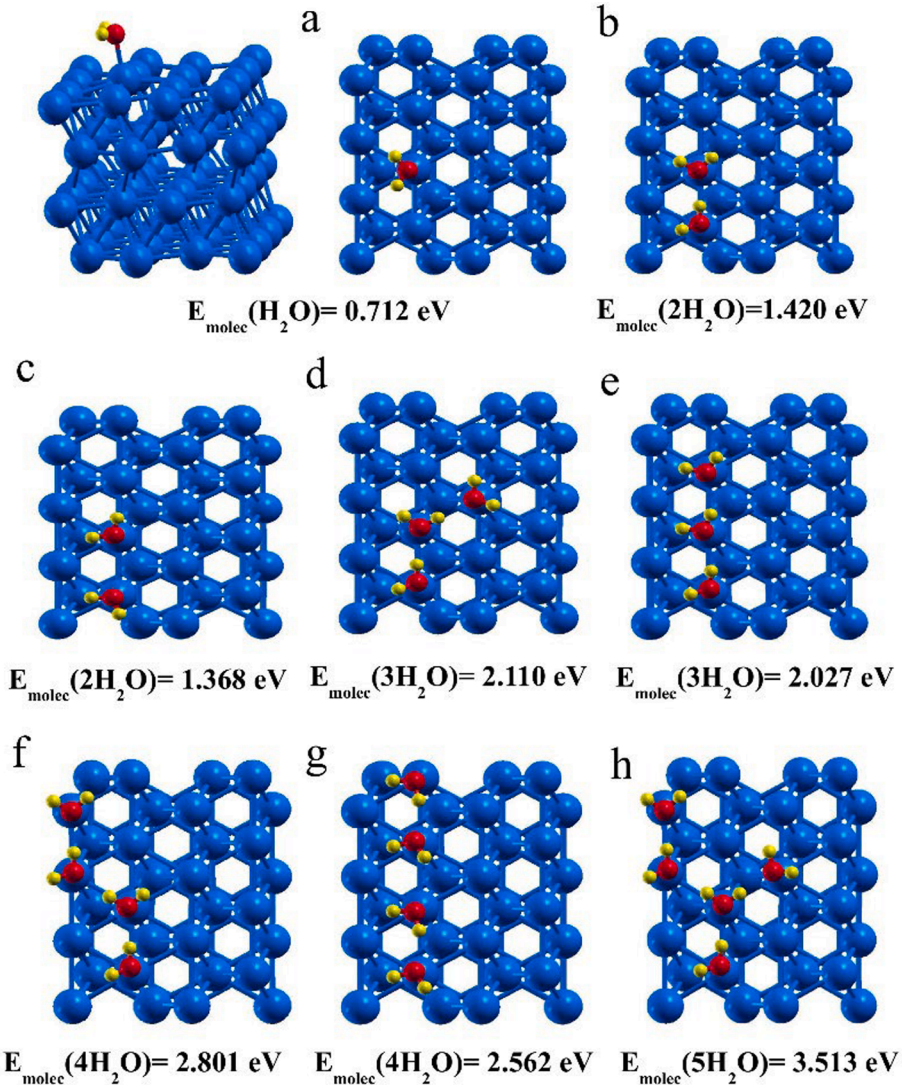

Fig. 8. Lowest energy structures (and a low-lying structure in some cases) for multiple adsorption of water molecules (n = 1–5) at the Zr surface. In each case, the total adsorption energy $E_{molec}[nH_2O]$ of the n H_2O molecules is given. Blue spheres: Zr atoms. Red spheres: O atoms. Yellow spheres: H atoms.

Table 5
Average adsorption energies per molecule, $E^{av}_{molec}[nH_2O]$, for adsorption of n = 1 – 8 water molecules on the surface of Zr, and adsorption energy of each newly added molecule, $E^{last}_{molec}[nH_2O]$. All energies in eV.

n	1	2	3	4	5	6	7	8
$E^{av}_{molec}[nH_2O]$	0.712	0.710	0.703	0.700	0.703	0.702	0.691	0.696
$E^{last}_{molec}[nH_2O]$	0.712	0.708	0.690	0.691	0.712	0.699	0.629	0.728

oxygen adatoms per unit cell. The most favorable adsorption positions are on hollow sites, and the O atoms show two bonding modes: either bonding to a single Zr atom, or bonding to a Zr and to a Pt atom. At this small coverage the interaction between O adatoms is small, and the total adsorption energy

$$E_{ads}[nO] = n\frac{1}{2}E[O_2] + E[\text{surface}] - E[nO \text{ on surface}] \quad (11)$$

which is included in Fig. 6, increases almost linearly with the number of O atoms.

In a Pt_3Zr surface covered with n fully dissociated water molecules (O+H+H) per cell, the energy required to recombine all the H atoms into H_2 molecules and desorb the n H_2 molecules can be calculated using the energies of the oxidized nO-Pt_3Zr surface and the n(O+H+H)-Pt_3Zr surface:

$$E_{desorp}[nH_2] = nE[H_2 \text{ gas}] + E[nO \text{ on surface}] - E[(nO + 2nH) \text{ on surface}]. \quad (12)$$

Table 4 shows those desorption energies for n = 1–3. At low coverage (n = 1), $E_{desorp}[H_2]$ = 1.313 eV. With increasing coverage of oxygen and hydrogen species (n = 2, 3), the total desorption energy of the n hydrogen molecules increases less than linearly with n. The average desorption energy $E^{av}_{desorp}[nH_2] = E_{desorp}[nH_2]/n$ decreases below 1 eV for increasing n.

Overall, the calculations predict that when water is adsorbed, the surface of the Pt_3Zr alloy will be preferentially saturated with hydroxyl OH groups bonded to the Zr surface atoms, and H atoms bonded to the Pt

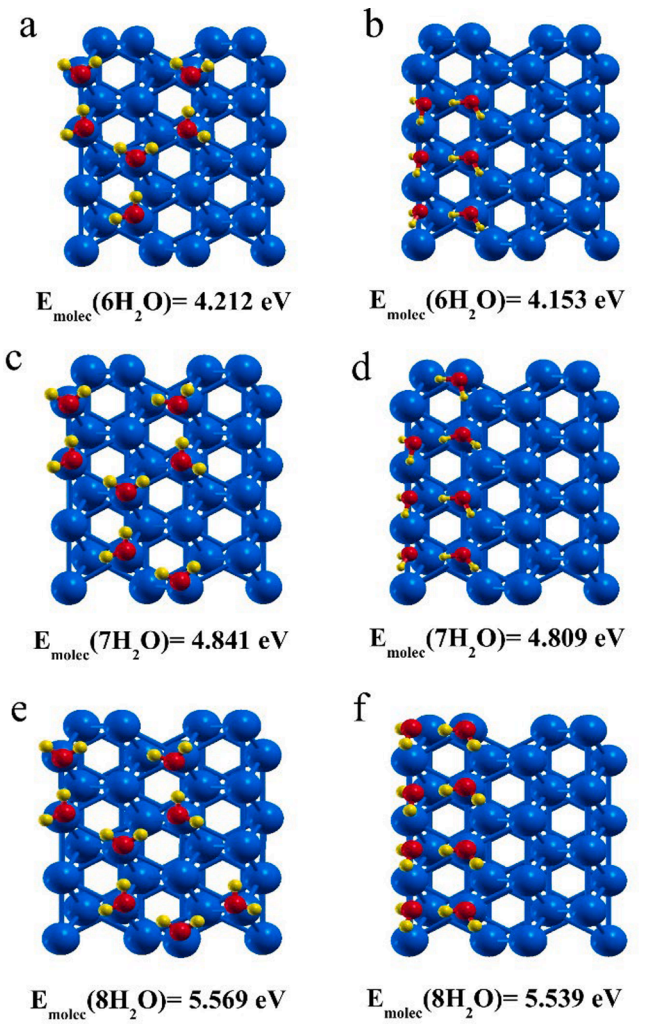

Fig. 9. Lowest energy structure (and one low-lying configuration) for multiple adsorption of water molecules (n = 6–8) at the Zr surface. In each case, the total binding energy $E_{molec}[nH_2O]$ of the n H_2O molecules is given. Blue spheres: Zr atoms. Red spheres: O atoms. Yellow spheres: H atoms.

surface atoms. The concentration of these species at the surface will be determined, at given pressure and temperature, not only by the relative stabilities with respect to adsorption of intact water or full dissociation into O and H, but also by the energy barriers to dissociate molecular water into OH and H, or into O and two H atoms. Fig. 7 shows the reaction barriers for the dissociation of H_2O first to OH+H and then to O+H+H on the Pt_3Zr surface. Dissociation of water into OH and H presents a moderate activation barrier of 0.41 eV. Then, from the most stable conformation of dissociated water (with a binding energy of 1.475 eV), breaking the O–H bond of the adsorbed hydroxyl group needs to overcome a much higher barrier of 1.18 eV. In addition, the final state in Fig. 7, with fully dissociated (O+H+H) water, is less stable than the state corresponding to intact hydroxyl (OH+H) on the surface by about 0.2 eV. Therefore, there is a strong resistance to break the O–H bond, and against total oxidation of the surface.

3.2. Water on the Zr surface

The adsorption of water molecules and their dissociation at the pure Zr(0001) surface has been investigated with the objective of comparing the results to those for the Pt_3Zr surface. Fig. 8 shows the most stable structure and some low lying conformations for the adsorption of up to five intact water molecules. The total adsorption binding energies $E_{molec}[nH_2O]$ are also given in the Figure (the definitions of $E_{molec}[nH_2O]$, $E^{av}_{molec}[nH_2O]$, and $E^{last}_{molec}[nH_2O]$ are the same as in equations (1), (2) and (3), just changing Pt_3Zr by Zr). For a single molecule, binding takes place in a conformation with the molecular plane nearly parallel to the surface and the oxygen atom bonded to a Zr atom at a distance of 2.33 Å. That specific Zr atom is lifted up by 0.4 Å from the plane of the Zr atoms in the surface layer. The binding energy of a single H_2O molecule to the surface is moderate, 0.71 eV, and it is slightly smaller than the corresponding binding energy at the Pt_3Zr surface (0.946 eV). The adsorption energy is consistent with the value of 0.62 eV calculated by Shuang-Xi Wang et al. [31] for adsorption of H_2O on the (0001) surface of Zr. When two intact water molecules are co-adsorbed at the Zr surface, these tend to form hydrogen bonds between them, while maintaining the O-Zr bonds. Interestingly, the strength of those hydrogen bonds is quite weak, as the comparison between the alternate conformations (b) and (c) show; when the hydrogen bond is not present because of the larger distance between the two water molecules (conformer c), the binding energy only decreases by 0.05 eV. The average adsorption energies per molecule $E^{av}_{molec}[nH_2O]$ and the adsorption energy of the last adsorbed molecule $E^{last}_{molec}[nH_2O]$ are given in Table 5. $E^{av}_{molec}[nH_2O]$ and $E^{last}_{molec}[nH_2O]$ have fairly constant values around 0.7 eV; that is, those adsorption energies do not show significant variations with the number of water molecules. This means that cooperative or competitive co-adsorption effects between water molecules are almost absent, and the surface will continue adsorbing water molecules until a full network of hydrogen bonded molecules occupies all the available sites. Those adsorption energies are a bit smaller than the corresponding adsorption energies on Pt_3Zr collected in Table 1.

Fig. 9 shows the lowest energy structure (and one low-lying configuration) for adsorption of six, seven and eight intact water molecules on the Zr surface. In each case, two alternative arrangements with nearly the same adsorption binding energies were found. In the first arrangement (conformations a, c, e) all the oxygen atoms are on top of Zr atoms, and all the water molecules form O ••• H hydrogen bonds. The competing arrangements (conformations b, d, f) have the water molecules distributed in two parallel rows; in one row, oxygen atoms are bound on top of Zr atoms, whereas the water molecules in the other row are detached from the Zr sites. The energetic cost of such detachment is compensated by the formation of shorter (and stronger) O ••• H hydrogen bonds between co-adsorbed water molecules.

Then, the dissociation of water molecules into hydroxyl OH groups and H atoms at the pure Zr surface was investigated. The results for one and two water molecules are shown in Fig. 10, and the different dissociative adsorption energies are defined as in equations (5), (6) and (7), just by changing Pt_3Zr to Zr. The OH groups are preferentially located at hollow sites between three surface Zr atoms, in an upright orientation. Let us note that there are two types of hollow sites at the Zr surface, one of them without a Zr atom below in the second layer (labelled here as site A), and a second type with a Zr atom in the second layer right below the hollow site (labelled as site B). It is observed in Fig. 10 that the OH groups prefer to occupy A sites. The detached H atoms also prefer to occupy hollow sites; however, with a small energy difference between sites A and B (0.04 eV in the case of a single adsorbed molecule). Panel d reveals that it is unfavourable for the H atom to approach the hydroxyl OH group at a neighbouring hollow site, with the binding energy decreasing by 0.34 eV with respect to the lowest energy conformation of panel a. The high dissociative adsorption energy for the most stable conformation, $E_{diss}[OH+O] = 3.48$ eV, indicates that water has a marked tendency towards dissociation at the pure Zr surface. With respect to H_2O adsorbed in molecular form (Fig. 8), a large energy gain of 2.7 eV in the adsorption energy is achieved upon breaking of the H-OH bond. Placing the H atom of Fig. 10a in a position embedded slightly below the surface has an energy cost of 0.58 eV, which is less than the calculated cost for the Pt_3Zr surface. For two coadsorbed dissociated H_2O molecules (Fig. 10 e) the total adsorption energy $E_{diss}[2(OH+O)]$ is very close to

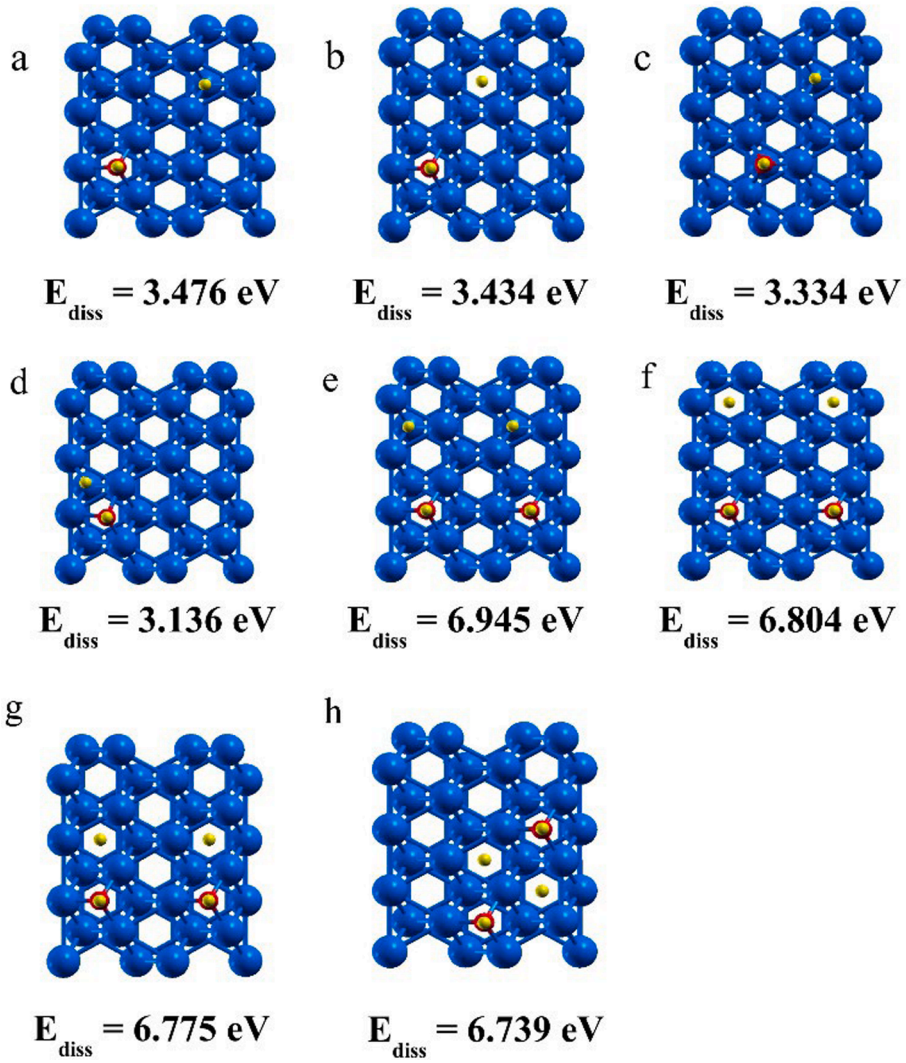

Fig. 10. Lowest energy structure and some low-lying adsorption configurations for one and two water molecules dissociated into OH and H at the Zr surface. In each case, the dissociative adsorption energy $E_{diss}[n(OH+O)]$ with respect to n gas phase H_2O molecules is given. Blue spheres: Zr atoms. Red spheres: O atoms. Yellow spheres: H atoms.

twice the adsorption energy of a single dissociated molecule, indicating that the interaction between the two dissociated molecules is almost negligible. This is not surprising, given the distance, of more than 5 Å, between the two coadsorbed molecules. Other alternative arrangements (panels f-h in Fig. 10) have similar adsorption energies to the ground state of panel e, all within 0.2 eV. The structures for larger coverages (three to five dissociated water molecules) are given in Fig. 11. A tendency to maximize the distances between OH groups and H atoms is observed, which leads, for $n = 5$, to clustering of OH and H in different regions of the cell. Again, as Table 6 shows, the dissociated water molecules do not interact strongly with each other, and the adsorption energy of each additional molecule, $E_{diss}^{last}[n(OH+H)]$, is fairly constant, decreasing by less than 10 % with respect to the value for the first adsorbed water molecule.

Finally, we have studied the full dissociative adsorption of water into H and O atoms at the pure Zr surface, and the results for one, two and three molecules per cell are shown in Fig. 12. The different dissociative adsorption energies are defined as in equations (8), (9) and (10), just by changing Pt_3Zr to Zr. For a single molecule, the most stable location of the O atom is at a hollow site of type A. As it happened for the dissociation of water into OH and H, detached hydrogen atoms show a preference for hollow sites of type B. The dissociative adsorption energy is 5.52 eV (in comparison to 3.48 eV in Fig. 10), revealing that 2 eV are gained upon dissociation of the adsorbed OH group into O and H atoms. When the H atoms move to other hollow sites (configurations 12b −12d) the energy changes only slightly, indicating that the H adatoms could easily diffuse around the surface. Configuration 12e shows that displacing the O adatom from a hollow site A to a hollow site B has a sizable energy cost of around 0.5 eV (with respect to the lowest energy configuration 12a). Then, we have examined the strenght of the bonding of the dissociated H atoms to the Zr surface. Panel 12f shows the relaxed geometry of a configuration with the O atom on its most stable adsorption site and the two H atoms recombined into an H_2 molecule weakly physisorbed on the surface. This conformation is less stable, by 2.2 eV, than the one with the two separated H atoms adsorbed on the surface, indicating that there is a substantial energy penalty for the recombination of the two H atoms and desorption of the formed H_2 molecule from the surface. Therefore, it is likely that, after complete splitting of water molecules, most of the atomic hydrogen will remain at the Zr surface or diffuse into the bulk. For two and three fully dissociated water molecules (configurations 12e-12 l) the total binding energy is nearly proportional to the number of molecules, meaning that saturation coverage has not been reached at $n = 3$. In contrast, for the Pt_3Zr surface, we found that saturation coverage is reached at $n = 2$. This confirms again that the pure Zr surface is significantly more reactive to water than the Pt_3Zr one.

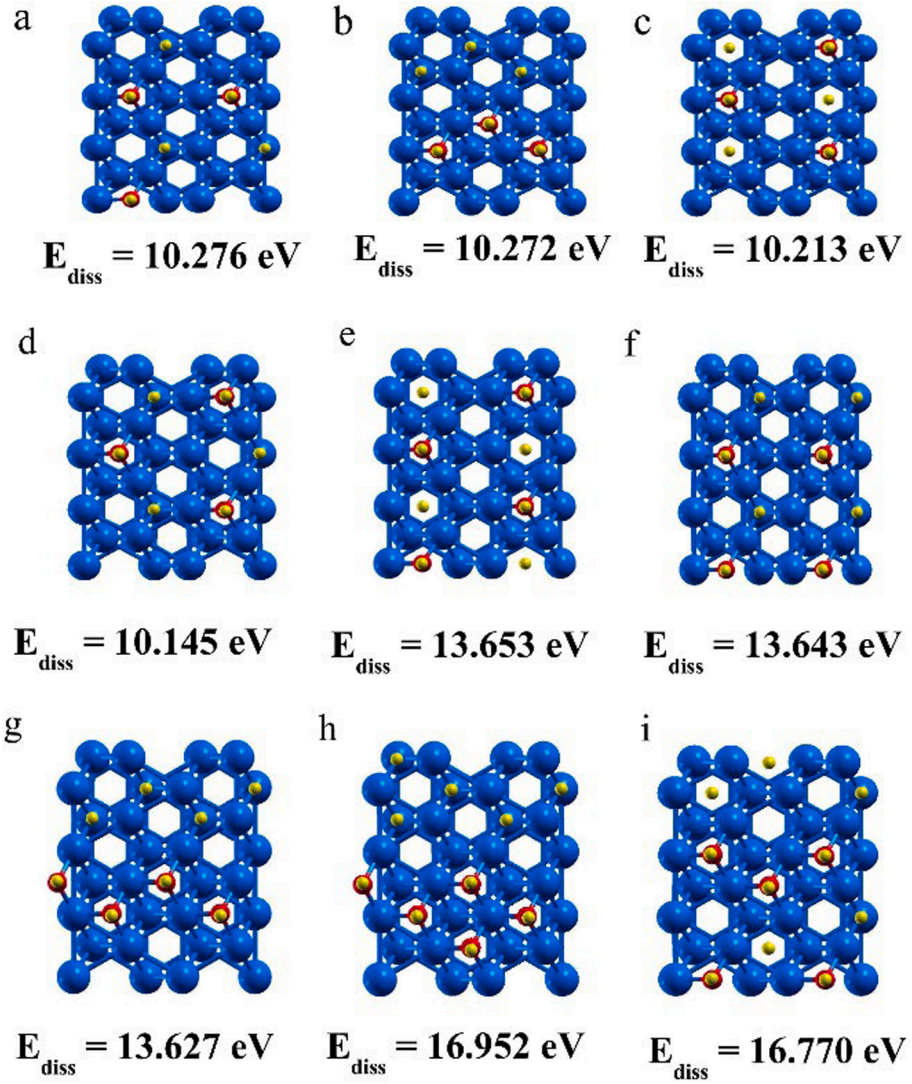

Fig. 11. Lowest energy structure and some low-lying adsorption configurations for $n = 3$–5 water molecules dissociated into OH and H at the Zr surface. In each case, the dissociative adsorption energy $E_{diss}[n(OH+O)]$ with respect to n gas phase H_2O molecules is given. Blue spheres: Zr atoms. Red spheres: O atoms. Yellow spheres: H atoms.

Table 6
Average adsorption energy per molecule, $E^{av}_{diss}[n(OH+H)]$ for the dissociative adsorption of $n = 1 - 5$ water molecules into OH and H on the Zr surface, and dissociative adsorption energy of each newly added water molecule, $E^{last}_{diss}[n(OH+H)]$. All energies in eV.

n	1	2	3	4	5
$E^{av}_{diss}[n(OH+H)]$	3.476	3.472	3.425	3.413	3.390
$E^{last}_{diss}[n(OH+H)]$	3.476	3.469	3.331	3.377	3.299

Multiple adsorption of oxygen atoms at the pure Zr surface has also been investigated. The most stable conformations found for $n = 1 - 7$ oxygen atoms are shown in Fig. 13. The O atoms prefer to occupy hollow sites of type A, which is consistent with the results in Fig. 12. The different adsorption energies are defined in this case

$$E_{ads}[nO] = n\frac{1}{2}E[O_2] + E[\text{surface}] - E[nO \text{ on surface}] \quad (13)$$

$$E^{av}_{ads}[nO] = E_{ads}[nO]/n \quad (14)$$

$$E^{last}_{ads}[nO] = \frac{1}{2}E[O_2] + E[(n-1)O \text{ on surface}] - E[nO \text{ on surface}] \quad (15)$$

The total adsorption energies $E_{ads}[nO]$, included in Fig. 13, are sizable. The average adsorption energies per O atom, $E^{av}_{ads}[nO]$, and the adsorption energy of the last added O atom, $E^{last}_{ads}[nO]$, are shown in Table 7. Up to four oxygen atoms, the adsorption energy of each new added O atom has an almost constant value of 5.8 eV (see Table 7). There is a small drop to a value of 5.5 eV for the fifth O atom, due to the need to locate oxygen adatoms at neighbouring locations in hollow sites of A type. Then, a nearly constant binding energy close to 5.5 eV is maintained up to the seventh O atom. For the Zr surface with up to three dissociated water molecules (O+H+H), the energy required to recombine the H atoms into H_2 molecules and detach the H_2 molecules from the surface is around 2.2 eV per molecule, a value much larger than the corresponding detachment energies from the Pt_3Zr surface. This again exhibits the higher reactivity of the pure Zr surface.

As we did in the case of the Pt_3Zr alloy, we have calculated the energy barriers for the complete dissociation of the H_2O molecule into O and H adatoms on the Zr surface. The two dissociation steps are independently shown in Fig. 14. The first step of the dissociation reaction involves breaking one O–H bond of the H_2O molecule, and the activation

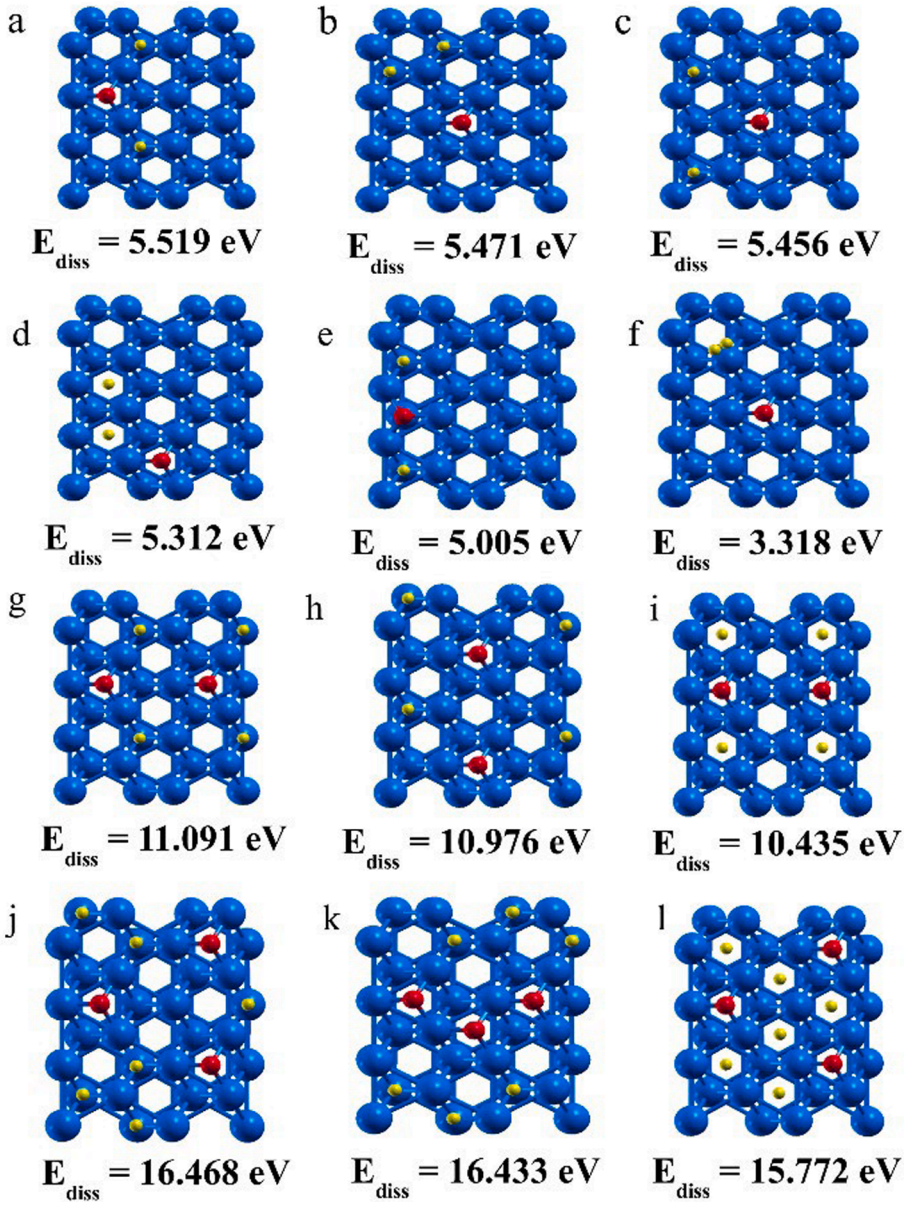

Fig. 12. Top views of the lowest energy structure, and several low-lying configurations for the full dissociative adsorption of one (conformers a − f), two (conformers g − i), and three (conformers j − l) water molecules at the Zr surface. In each case, the total dissociative adsorption energy $E_{diss}[n(O+H+H)]$ with respect to n gas phase molecules (n = 1, 2, 3) is given. Blue spheres: Zr atoms. Red spheres: O atoms. Yellow spheres: H atoms.

barrier is small, 0.30 eV. The transition state is characterized by a distorted orientation of the water molecule, in which the dissociating H atom builds up a bond with the underlying Zr atom. To study the second dissociation step we start with the lowest energy configuration of OH+H, that in Fig. 10a. The activation barrier for breaking the O–H bond in the hydroxyl group amounts to 0.56 eV. Although a bit larger than the barrier of the first dissociation step, it is still moderate, meaning that even at not too high temperatures adsorbed hydroxyls could decompose into oxygen and hydrogen adatoms, promoting the formation of a superficial oxide layer.

Comparing the results obtained for water dissociation on the pure Zr surface with those for dissociation on the Pt_3Zr alloy, important differences can be noticed. First, the reactions for complete water dissociation proceed with very small activation barriers on the Zr surface, while in the case of Pt_3Zr the step of dissociating the O–H bonds has a barrier larger than 1 eV, difficult to surpass. Second, in the case of pure Zr, the stability of water completely dissociated into O+H+H atoms is much higher (by around 2 eV) than the stability of the partially dissociated H+OH intermediate. This situation is reversed for the Pt_3Zr alloy, where the partially dissociated H+OH state is more stable than the state with separated O and H adatoms. Finally, after complete water dissociation, the coadsorbed H adatoms are more strongly bound to the surface in the case of pure Zr. The energy required to recombine two H atoms on the Zr surface and desorb the formed H_2 molecule is about twice the value for the same process on the Pt_3Zr surface.

3.3. Analysis of the electronic structure

To gain a better understanding on the different reactivity of the Zr and Pt_3Zr surfaces, we have analyzed in detail the electronic structure and bonding characteristics of water dissociated into OH and H. In panels a) and b) of Fig. 15, we show the Bader atomic charges [32,33] at some selected surface atoms. In the case of pure Zr, the bare Zr surface atoms have small negative charges of around −0.15 e. But, when we consider Zr atoms bonded to either OH or H, those atoms become positively charged, with charges in the range of + 0.14 e to + 0.24 e.

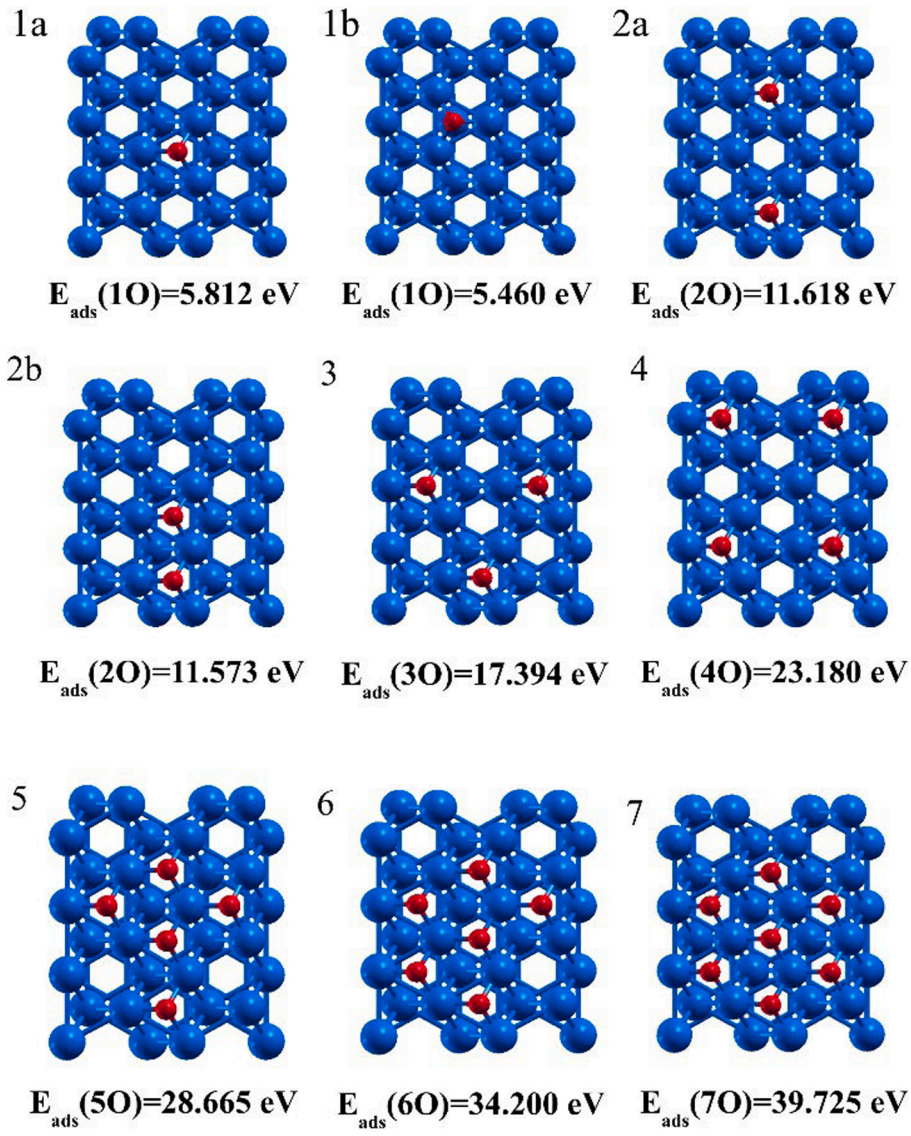

Fig. 13. Top views of the lowest energy structure for multiple adsorption of oxygen atoms (n = 1–7) at the pure Zr surface. A low-lying configuration is also shown for one and two adsorbed O atoms. In all cases, the total binding energy with respect to gas-phase O_2 molecules, $E_{ads}[nO]$, is given. Blue spheres: Zr atoms. Red spheres: O atoms. Yellow spheres: H atoms.

Table 7
Average adsorption energy per O atom, $E^{av}_{ads}[nO]$, for the adsorption of one to seven O atoms on the Zr surface, and adsorption energy of each newly added O atom, $E^{last}_{ads}[nO]$. All energies in eV.

n	1	2	3	4	5	6	7
$E^{av}_{ads}[nO]$	5.812	5.809	5.798	5.795	5.733	5.700	5.675
$E^{last}_{ads}[nO]$	5.812	5.806	5.776	5.786	5.485	5.535	5.525

This is caused by the fact that both the OH group and the H atom draw some electronic charge from those Zr atoms. The H atom has a charge of −0.70 e, and the O atom of the OH group has a charge of −1.33 e (which, of course, also includes the charge transferred by the H atom within the hydroxyl).

In the Pt_3Zr alloy, the metal atoms at the surface are charged because of the ionicity of this alloy. Bare Zr atoms on the surface have positive charges close to + 1.75 e, arising from electron transfer from Zr to Pt atoms due to the higher electronegativity of Pt [34]. The surface Pt atoms which are not bonded to adsorbates have negative charges of approximately −0.60 e. The oxygen atom of the OH group has an extra charge of −1.14 e, lower in comparison to its charge of −1.33 e in the Zr surface, because the Zr atoms are already substantially charged in Pt_3Zr and cannot deliver much more charge. Consequently, the oxygen-surface interaction in Pt_3Zr is weaker than in the pure Zr metal. The most important difference, when comparing the Pt_3Zr and Zr surfaces, resides in the charge gained by the dissociated H atom. At the Pt_3Zr surface, the charge of the H atom is −0.14 e, much lower than the charge of −0.70 e on the pure Zr surface. The reason for this behavior is that in the Pt_3Zr surface the H atom is bonded to Pt atoms, which are more electronegative than the Zr atoms.

The total electronic densities of states (DOS) for both surfaces are shown in panel c) of Fig. 15. Partial densities of states (PDOS), that is, the DOS projected on the hydrogen s and oxygen s and p orbitals, and in the Pt_3Zr case also projected on the Zr s and d states, are also included. The DOS and PDOS corresponding to OH+H on the Pt_3Zr surface clearly reflect the ionic contribution to the Pt-Zr bonding; most of the Zr states are located at energies above the Fermi level, and therefore some electronic charge is transferred to the Pt d-band, which becomes almost filled; indeed, a sizable energy gap of 0.5 eV appears just above the top

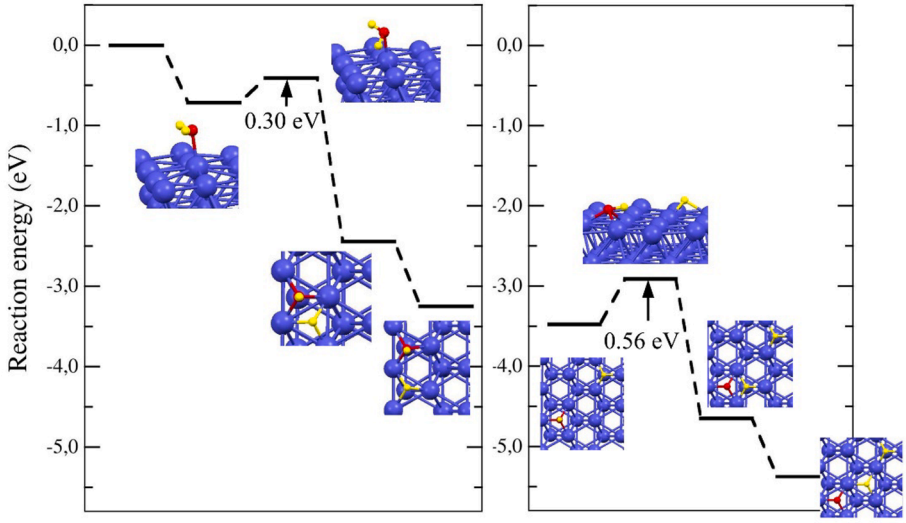

Fig. 14. Intermediate steps and reaction barriers for the complete dissociation of an H_2O molecule at the pure Zr surface. The left panel shows the dissociation into OH and H, and the second shows the dissociation of OH into O and H. The energies in the two panels are aligned in the same scale.

of the platinum *d*-band. The positions of the electronic states corresponding to the oxygen 2*p* levels and the 1*s* level of the dissociated hydrogen are explicitly indicated. Then, in panels d) and e), three-dimensional contours showing the spatial distribution of the real part of those electronic states are plotted (blue and red surfaces indicate, respectively, regions of positive and negative phase of the wave functions). In the case of Pt_3Zr, the Op_x and Op_y levels are broadened (see panel c) due to the hybridization with the surface Pt states. Indeed, the corresponding wave function plots reveal mixing with *d* states of Zr and Pt atoms, even with those atoms which are not close neighbors of the OH group. The Op_z state is more localized, being only hybridized with the *d* states of the Zr atom located directly below the OH group.

The comparison between the two surfaces reveals that the oxygen 2*p* states are spatially more localized in the case of pure Zr. Also, they are shifted to more negative (more strongly bound) energies, with respect to the Fermi level. This indicates that the O-Zr interaction is stronger for the pure Zr surface, and this is confirmed by all the calculations presented in Sections 3.1 and 3.2 (compare, for instance, Figs. 6 and 13). The wave function plots for the pure Zr surface in panel e) also show a localized hydridization between oxygen 2*p* states and the *d* states of the neighbouring Zr atoms. This is also true for the 1*s* state of the dissociated H. Upon interaction with the Zr atoms, this state is splitted into two states close in energy, with the wave functions partially localized in both the H atom and the Zr atoms below it.

3.4. *Effect of the temperature*

The calculations performed do not take into account the high temperature in the region of contact between water and the cladding surface. However, some reasonable arguments can be offered on the effect of the temperature. Pt_3Zr is a high-temperature structural material with high structural and thermal stability [35–37]. Its melting temperature is 2250 °C, well above the temperatures in the cladding that contains the fissionable material and the water of the primary circuit of the nuclear reactor, which is the water in contact with the cladding surface. Those temperatures range between 290 °C and 325 °C. - It is unlikely that the structural integrity of the Pt_3Zr cladding will suffer at those temperatures. The high temperature facilitates the dissociation of H_2O into OH and H on the surface of the cladding, more in the case of Zr (the activation barrier for dissociation is 0.30 eV) than in Pt_3Zr (the activation barrier is larger, 0.41 eV). The high temperature may also facilitate the additional dissociation of OH into O and H on the Zr surface (the activation barrier is 0.56 eV). This is less likely on the Pt_3Zr surface. First, because the activation barrier is larger (1.18 eV). But, more important, because the activation barrier for the recombination of OH and H back into H_2O is 0.96 eV (see Fig. 7). This recombination barrier is smaller than 1.18 eV, and recombination will be somehow more favorable than the dissociation of OH into O and H. The high temperature may also enhance the diffusion of H atoms towards the bulk of the alloy. Although this process has not been studied in this work, we can get insight from the calculations performed. Diffusion of H atoms between adjacent Pt-Pt bridge positions on the surface of Pt_3Zr is likely to occur at high temperatures (the data in Fig. 2 show that the energy differences between different configurations of the H atom on the surface are small, about 0.1 eV). However, the more relevant diffusion into the bulk is less likely. In the case of water dissociation into OH and H on the surface of Pt_3Zr, we explored a configuration with the H atom embedded below the most external layer of Pt atoms (see panel f of Fig. 2). That configuration is the least stable one in Fig. 2, and in particular is less stable than the conformer of panel a) by 0.7 eV. So, diffusion barriers towards the bulk of the Pt_3Zr cladding will be most likely larger than 0.7 eV, and the tendency to diffuse towards the bulk of the cladding will also compete with the tendency to recombine H and OH.

4. Conclusions

The adsorption and interaction of water with the surfaces of Pt_3Zr and Zr has been investigated using density functional theory. Molecular H_2O occupies adsorption sites on top of the Zr atoms of the Pt_3Zr surface with adsorption energies close to 0.9 eV/molecule, until those sites are saturated. Additional H_2O molecules occupy sites on top of Pt atoms, and the binding energies decrease. In the case of the pure Zr surface, the molecular adsorption energies of H_2O are a bit smaller. In both surfaces, hydrogen bonds form between the water molecules as the coverage increases.

Dissociative adsorption of water is energetically favored against molecular adsorption, but important differences between the two surfaces are predicted. Dissociative adsorption of H_2O molecules into OH and H, and also full dissociation into O and two H atoms were considered. The dissociation into OH and H is favored on the Pt_3Zr surface, but saturation effects appear when all the surface Zr atoms are covered by OH. The activation barriers for dissociation of H_2O on the Pt_3Zr surface are sizable, in particular the barrier for the OH→O+H process, which amounts to 1.2 eV. The dissociation of H_2O molecules is easier on the pure Zr surface: the dissociative adsorption energies (into OH+H, or into O+H+H) are much larger than on Pt_3Zr, and the activation barriers for

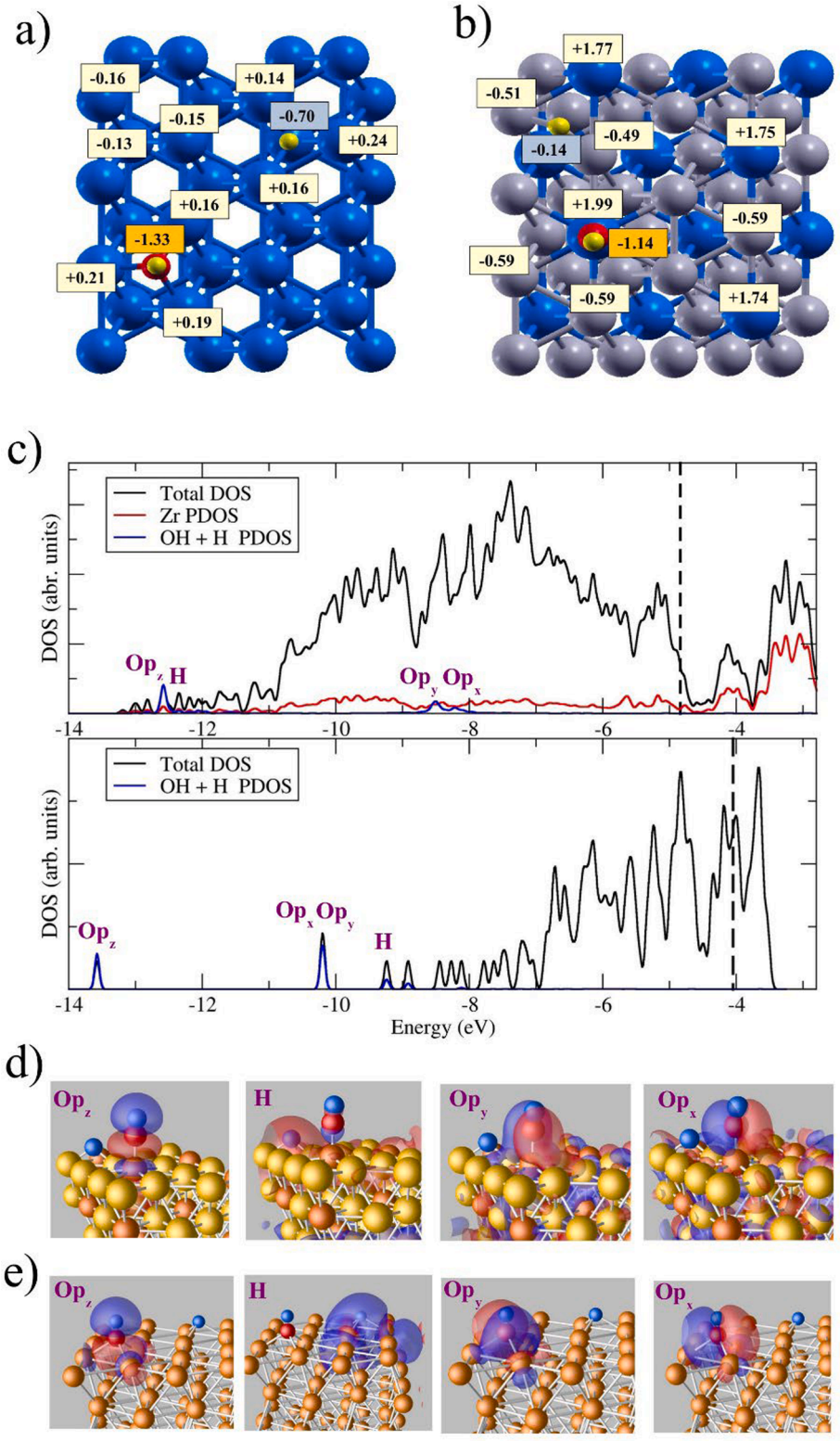

Fig. 15. a) Bader charges (in e units) at selected atoms for water dissociated into - OH and - H at the pure Zr surface (a), and the Pt_3Zr surface (b). c) Comparison of electronic densities of states (DOS) for the case of a single water molecule dissociated into OH and H at the Pt_3Zr and pure Zr surfaces. d) Three dimensional surfaces with constant value of the one-electron wave functions for oxygen and hydrogen states at the Pt_3Zr surface. Blue and red contours indicate, respectively, regions of positive and negative phase of the wave functions. e) The same for the pure Zr surface.

dissociation are significantly smaller. Full dissociation into O+H+H is energetically preferred on the Zr surface. Embedding of atomic H below the Pt_3Zr surface is unfavorable with respect to staying above the surface, but this is easier on pure Zr.

The energies required for the recombination of H atoms into H_2 molecules and desorption of those molecules from the Zr surface are larger, by a factor of two, compared to the same process on the Pt_3Zr surface. In summary, the results reported in - this work provide evidence

for the significantly larger reactivity of the Zr surface with water, as compared to the Pt_3Zr surface. The decomposition of water molecules into H and OH (or O+H+H), and the penetration of H into the bulk are more difficult on Pt_3Zr. The recombination of H atoms into H_2 and desorption of the H_2 molecules from the surface is easier on Pt_3Zr. Thus, Pt_3Zr could provide a good protective coating of different Zr parts of nuclear reactors, that would diminish the oxidation and the diffusion of hydrogen into the bulk of the walls, and the corresponding weakening of their strength.

CRediT authorship contribution statement

J.S. Arellano: Writing – review & editing, Writing – original draft, Visualization, Investigation, Formal analysis, Conceptualization. **L.M. Molina:** Writing – review & editing, Writing – original draft, Visualization, Investigation, Formal analysis, Conceptualization. **M.J. López:** Writing – review & editing, Writing – original draft, Investigation, Formal analysis, Conceptualization. **J.A. Alonso:** Writing – review & editing, Writing – original draft, Investigation, Formal analysis, Conceptualization.

Declaration of competing interest

The authors declare that they have no known competing financial interests or personal relationships that could have appeared to influence the work reported in this paper.

Data availability

Data will be made available on request.

Acknowledgements

Work supported by Ministerio de Ciencia e Innovación of Spain (Grants PID2019-104924RB-I00 funded by MCIN/AEI/ 10.13039/501100011033, and PID2022-138340OB-I00 funded by MCIN/AEI/ 10.13039/501100011033 and FSE+), and the University of Valladolid (GIR Nanostructure Physics). J.S.A. gratefully acknowledges the computing time provided at the LSVP at UAM-Iztapalapa, and J.A.A acknowledges the hospitality of DIPC.

Appendix A. Supplementary data

Supplementary data to this article can be found online at https://doi.org/10.1016/j.commatsci.2024.113313.

References

[1] F. Cattant, D. Crusset, D. Féron, Corrosion issues in nuclear industry today, Mater. Today 11 (2008) 32–37.
[2] A.T. Motta, A. Couet, R.J. Comstock, Corrosion of zirconium alloys used for nuclear fuel cladding, Ann. Rev. Mater. Res. 45 (2015) 311–343.
[3] B. Cox, Some thoughts on the mechanisms of in-reactor corrosion of zirconium alloys, J. Nuclear Materials 336 (2005) 331–368.
[4] P. Rudling, Zr alloy corrosion and hydrogen pickup, ANT International, Molnlycke, Sweden, 2013.
[5] I. Bespalov, M. Datler, S. Buhr, W. Drachsel, G. Rupprechter, Y. Suchorski, Initial stages of oxide formation on the Zr surface at low oxygen pressure: An in situ FIM and XPS study, Ultramicroscopy 159 (2015) 147–151.
[6] J.L. Vandegrift, P.M. Price, J.P. Stroud, C.J. Parga, I.J. Van Rooyen, B.J. Jaques, D. P. Butt, Oxidation behavior of zirconium, zircaloy-3, zircaloy-4, Zr-1Nb, and Zr-2.5Nb in air and oxygen, Nuclear Materials and Energy 20 (2019) 100692–100699.
[7] T.W. Chiang, A. Chernatynskiy, M.J. Noordhoek, S.B. Sinnott, S.R. Phillpot, Anisotropy in oxidation of zirconium surfaces from density functional theory calculations, Comput. Mater. Sci. 98 (2015) 112–116.
[8] Y.M. Wang, Y.S. Li, K.A.R. Mitchell, A LEED crystallographic analysis for the half monolayer structure formed by O at the Zr(0001) surface, Surf. Sci. 342 (1995) 272–280.
[9] F.H. Wang, S.Y. Liu, J.X. Shang, Y.S. Zhou, Z. Li, J. Yang, Oxygen adsorption on Zr (0001) surfaces: Density functional calculations and a multiple-layer adsorption model, Surf. Sci. 602 (2008) 2212–2216.
[10] K. Griffiths, C.S. Zhang, P.R. Norton, The autocatalytic decomposition of water on Zr(0001), Surf. Sci. 384 (1997) 70–80.
[11] R.K. Siripurapu, B. Szpunar, J.A. Szpunar, Molecular dynamics study of hydrogen in α-zirconium, Int. J. Nuclear Energy (2014) 912369.
[12] A. Zieliński, S. Sobieszczyk, Hydrogen-enhanced degradation and oxide effects in zirconium alloys for nuclear applications, Int. J. Hydrogen Energy 36 (2011) 8619–8629.
[13] B. Ensor, A.M. Lucente, M.J. Frederick, J. Sutliff, A.T. Motta, The role of hydrogen in zirconium alloy corrosion, J. Nuclear Materials 496 (2017) 301–312.
[14] K. Horáková, S. Cichoň, J. Lančok, I. Kratochvílová, L. Fekete, P. Sajdl, A. Krausová, J. Macák, V. Cháb, Corrosion protection of zirconium surface based on Heusler alloy, Pure Appl. Chem. 89 (2017) 553–563.
[15] C. Anghel, G. Hultquist, M. Limbäck, P. Szakalos, Effects of Pt surface coverage on oxidation of Zr and other materials, J. ASTM Internat. 5 (2008) N2.
[16] J. Zhang, Y. Shen, H. Wang, Q. An, Bi-doped zirconium alloys with enhanced water oxidation resistance, J. Phys. Chem. C 124 (2020) 23116–23125.
[17] J.K. Stalick, R.M. Waterstrat, The zirconium–platinum phase diagram, J. Alloys Comp. 430 (2007) 123–131.
[18] Y. Pan, S. Wang, L. Jia, X. Zhang, First-principles study of a new structure and oxidation mechanism of Pt_3Zr, RSC Adv. 7 (2017) 54772–54778.
[19] H. Li, J. Choi, W. Mayr-Schmölzer, C. Weilach, C. Rameshan, F. Mittendorfer, J. Redinger, M. Schmid, G. Rupprechter, Growth of an ultrathin zirconia film on Pt_3Zr examined by high-resolution X–ray photoelectron spectroscopy, temperature-programmed desorption, scanning tunneling microscopy, and density functional theory, J. Phys. Chem. C 119 (2015) 2462–2470.
[20] M. Antlanger, W. Mayr-Schmölzer, J. Pavelec, F. Mittendorfer, J. Redinger, P. Varga, U. Diebold, M. Schmid, $Pt_3Zr(0001)$: A substrate for growing well-ordered ultrathin zirconia films by oxidation, Phys. Rev. B 86 (2012) 035451.
[21] P. Lackner, J. Hulva, E.M. Köck, W. Mayr-Schmölzer, J. Choi, S. Penner, U. Diebold, F. Mittendorfer, J. Redinger, B. Klötzer, G.S. Parkinson, M. Schmid, Water adsorption at zirconia: from the $ZrO_2(111)/Pt_3Zr(0001)$ model system to powder samples, J. Mater. Chem. A 6 (2018) 17587–17601.
[22] A. Ruiz Puigdollers, G. Pacchioni, Reducibility of ZrO_2/Pt_3Zr and ZrO_2/Pt 2D films compared to bulk zirconia: a DFT+U study of oxygen removal and H_2 adsorption, Nanoscale 9 (2017) 6866–6876.
[23] W. Kohn, L.J. Sham, Self-consistent equations including exchange and correlation effects, Phys. Rev. 140 (1965) A1133–A1138.
[24] J.P. Perdew, K. Burke, M. Ernzerhof, Generalized gradient approximation made simple, Phys. Rev. Lett. 77 (1996) 3865–3868.
[25] J. Enkovaara, C. Rostgaard, J.J. Mortensen, J. Chen, M. Dulak, L. Ferrighi, J. Gavnholt, C. Glinsvad, V. Haikola, H.A. Hansen, et al., Electronic structure calculations with GPAW: a real-space implementation of the projector augmented-wave method, J. Phys. Condens. Matter. 22 (2010) 253202.
[26] D.C. Liu, J. Nocedal, On the limited memory BFGS method for large scale optimization, Math. Program. 45 (1989) 503–528.
[27] A. Alavi, P. Hu, T. Deutsch, P.L. Silvestrelli, J. Hutter, CO oxidation on Pt(111): an Ab initio density functional theory study, Phys. Rev. Lett. 80 (1998) 3650–3653.
[28] L. Kristinsdóttir, E. Skúlason, A systematic DFT study of hydrogen diffusion on transition metal surfaces, Surf. Sci. 606 (2012) 1400–1404.
[29] S.M. Sharada, R.K.B. Karlsson, Y. Maimaiti, J. Voss, T. Bligaard, Adsorption on transition metal surfaces: Transferability and accuracy of DFT using the ADS41 dataset, Phys. Rev. B 100 (2019) 035439.
[30] P. Ferrin, S. Kandoi, A.U. Nilekar, M. Mavrikakis, Hydrogen adsorption, absorption and diffusion on and in transition metal surfaces: A DFT study, Surf. Sci. 606 (2012) 679–689.
[31] Shuang-Xi Wang, Ping Zhang, Peng Zhang, Jian Zhao, Shu-Shen Li, Adsorption and dissociation of H_2O on Zr (0 0 0 1) with density-functional theory studies, J. Nuclear Materials 424 (212) 51–56.
[32] R.F.W. Bader, Atoms in Molecules - A Quantum Theory, Oxford University Press, Oxford, 1990.
[33] W. Tang, E. Sanville, G. Henkelman, A grid-based Bader analysis algorithm without lattice bias, J. Phys.: Cond. Mater. 21 (2009) 084204.
[34] J.A. Alonso, L.A. Girifalco, Electronegativity scale for metals, Phys. Rev B 19 (1979) 3889–3895.
[35] W. Metiri, K. Cheikh, Ab initio study of structural, electronic, thermo-elastic and optical properties of Pt_3Zr intermetallic compound, Chin. Phys. B 29 (2020) 047101.
[36] Z. Li, K. Xiong, Y. Sun, C. Jin, S. Zhang, J. He, Y. Mao, First-principles study of mechanical and thermodynamic properties of intermetallic Pt3M (M = Al, Hf, Zr Co, Y, Sc), Comput. Condensed Matter 23 (2020) e00462.
[37] Y. Pan, Experimental and theoretical investigation of origin of mechanical properties and facture mechanism of Pt_3Zr high-temperature material, JOM 72 (2020) 2419–2425.